

# Luminous early-type field galaxies at $z \sim 0.4$ – II. Star-formation history and space density

J.P. Willis,<sup>1\*</sup> P.C. Hewett<sup>2</sup>, S.J. Warren<sup>3</sup> and G.F. Lewis<sup>4</sup>

<sup>1</sup>*Departamento de Astronomía y Astrofísica, P. Universidad Católica, Avenida Vicuña Mackenna 4860, Casilla 306, Santiago 22, Chile*

<sup>2</sup>*Institute of Astronomy, Madingley Road, Cambridge CB3 0HA*

<sup>3</sup>*Blackett Laboratory, Imperial College of Science Technology and Medicine, Prince Consort Road, London SW7 2BZ*

<sup>4</sup>*Anglo-Australian Observatory, P.O. Box 296, Epping, NSW 1710, Australia*

Accepted YYYY monthname DD. Received YYYY monthname DD; in original form YYYY monthname DD

## ABSTRACT

We present a combined photometric and spectroscopic analysis of the star formation history and space density of a sample of 485 luminous,  $M_V - 5 \log h < -20.5$ , field early-type galaxies at redshifts  $0.3 \lesssim z \lesssim 0.6$ . The observed *b<sub>J</sub>ori* colours as a function of redshift, mean absorption line strengths and [OII] 3727 emission properties are used to constrain the star formation history of the galaxies. The mean star formation history of the early-type galaxy sample is consistent with an old ( $z_f > 1$ ), passively evolving luminosity-weighted stellar population. Twenty-one percent of the sample possess detectable [OII] 3727 emission consistent with a low level ( $\lesssim 1 \text{ M}_\odot \text{ yr}^{-1}$ ) of on-going star formation. Parametric and non-parametric estimates of the space density of the sample are derived. The integrated luminosity density at  $z \simeq 0.4$ , allowing only for passive luminosity evolution, is in excellent agreement with the local, ( $\langle z \rangle = 0.1$ ), luminosity density of early-type galaxies. Overall, the sample properties are consistent with a galaxy formation scenario in which the majority of luminous field early-type galaxies formed at redshifts  $z > 1$  and have largely evolved passively since the formation epoch.

**Key words:** early-type galaxies – luminosity function: star formation.

## 1 INTRODUCTION

The star-formation history and space density of luminous early-type galaxies in field<sup>†</sup> and cluster environments at significant cosmological look-back times place strong constraints upon theories of galaxy formation and evolution. Within the class of hierarchical formation models, early-type galaxies are predicted to result from a combination of major galaxy mergers (i.e. those involving roughly equal mass progenitors) together with the accretion of lower mass galaxies (Baugh, Cole & Frenk 1996; Kauffmann 1996). The merger rate and thus the production rate of early-type galaxies is predicted to be a strong function of local galaxy density; early-type galaxies in clusters arise from an early cosmic epoch of rapid merging and intense star formation whereas field early-type galaxies arise from a more protracted period of merging and star formation extending to redshifts  $z \lesssim 1$ . Thus, in hierarchical models, field early-

type galaxies are predicted to display lower mean ages and a greater dispersion in star formation history with respect to cluster early-type galaxies. For example, Kauffmann (1996) reports that cluster elliptical galaxies (i.e. those located within parent halos of mass  $10^{15} \text{ M}_\odot$ ) display luminosity weighted stellar ages between 8 and 12.5 Gyr compared to “field” elliptical galaxies (i.e. those located within parent halos of mass  $10^{13} \text{ M}_\odot$ ) displaying stellar ages between 6 and 11 Gyr. These predictions contrast with those resulting from models in which early-type galaxies observed in both field and cluster environments formed from the monolithic collapse of galaxy-mass (i.e.  $10^{11} - 10^{12} \text{ M}_\odot$ ) overdensities at early cosmic times (Larson 1974). The stellar populations in such galaxies are predicted to have formed in an early, largely coeval, burst of star formation and to have evolved passively since that time.

A important link between theoretical predictions and the observed properties of early-type galaxies is achieved via studies of the Fundamental Plane (hereafter FP) formed by such objects. Studies of the FP for luminous early-type galaxies in clusters now extend to redshifts  $z \sim 0.5$  (e.g. Pahre, Djorgovski & de Carvalho 1998; Jørgensen et al. 1999). The observed evolution of the FP parameters versus

\* Present address: European Southern Observatory, Alonso de Cordoba 3107, Vitacura, Casilla 19001, Santiago 19, Chile.

† Throughout this paper, “field” is taken to indicate regions outside rich galaxy clusters.

redshift in accordance with the predictions of a passively evolving stellar population, combined with a low intrinsic dispersion among the galaxies, imply that the majority of early-type galaxies in rich clusters formed at some early ( $z > 2$ ), coeval epoch. Further evidence that luminous early-type galaxies in rich clusters are composed of uniformly old stellar populations is derived from the observation that these galaxies display impressively uniform colours over the redshift interval  $0 < z < 1$  (Bower et al. 1992; Ellis et al. 1997; Stanford, Eisenhardt & Dickinson 1998). The exceptionally narrow range of colours displayed both internally, and between clusters, at significant cosmological look-back times ( $\sim 8$  Gyr) strongly supports an early, coeval formation epoch.

Given the relative abundance of data available for early-type galaxies in rich clusters at redshift  $z \sim 0.5$ , the generation of samples of field early-type galaxies with which to test the central predictions of galaxy formation theories is of considerable interest. Initial attempts to form the FP relation for distant field early-type galaxies (van Dokkum et al. 2001; Treu et al. 2001) indicate that field early-type galaxies exhibit an FP relation similar in the mean to that observed in rich clusters but displaying an increased scatter about the mean relation. These studies are limited by small sample sizes ( $\sim 20$  galaxies) and include galaxies over an extended redshift interval,  $0.1 < z < 0.5$ , leading to a degree of uncertainty due to the need for evolutionary corrections required to bring the galaxies to a common epoch.

The formation of early-type field galaxies via hierarchical merging also implies that their number density should be a strong function of look-back time (Kauffman, Charlot & White 1996). However, the failure to demonstrate any deficit in the number density of luminous field spheroidal galaxies at redshifts  $z < 1$  compared to local studies places strong constraints upon the proposed epoch of hierarchical merging (Schade et al. 1999). It is important to note however, that linking the predictions of numerical models directly to observations is hindered by uncertainties associated with galaxy classification (e.g. Abraham 1999).

Differences between the star-formation history of galaxies in field and cluster environments are likely to be augmented by the fact that the environment of rich clusters appears to actively suppress on-going/recent star-formation. In a study of 10 distant ( $z \sim 0.5$ ), rich clusters Dressler et al. (1999) and Poggianti et al. (1999) report that 20% of galaxies possess so-called “post-starburst”, (a+k), spectra, indicative of a recent cut-off in star-formation activity combined with an old stellar population. The frequency of the a+k class in a comparable field sample is considerably lower ( $\lesssim 4\%$ ), although the significance of this result is low given the small size of the field sample. However, the idea that star-formation activity in rich cluster galaxies is either suppressed (via ram-pressure stripping of neutral gas) or rapidly increased at early times (via galaxy-galaxy interactions and mergers) leading to exhaustion of the available gas supply, remains compelling.

While the advent of the Sloan Digital Sky Survey has recently allowed the definition of very large samples of early-type galaxies (Eisenstein et al. 2001, Bernardi et al. 2002) most existing studies of luminous early-type field galaxies over the redshift interval  $0 < z < 1$  have been confined to small numbers of objects present in galaxy redshift surveys

**Table 1.** Photometric selection criteria.

16.5	<	$m_i$	<	18.95
2.15	<	$b_J - or$	<	3.00
		$or - i$	<	1.05
2.95	<	$b_J - i$		

designed to constrain the global properties of the galaxy population, e.g. the Canadian Network for Observational Cosmology field galaxy redshift survey (CNOC; Yee, Ellingson & Carlberg 1996), the Canada France Redshift Survey (Hammer et al. 1997), and the AUTOFIB galaxy redshift survey (Heyl et al. 1997). Given the under representation of luminous early-type field galaxies in current galaxy surveys we have obtained multi-colour photometry and medium resolution optical spectroscopy for a large, well-defined sample of distant, luminous early-type field galaxies (Willis, Hewett & Warren 2001, hereafter Paper I). The observational data is of sufficient quality to place strong constraints on the star formation history and space density evolution of the population. By obtaining data for field galaxies with redshifts and luminosities comparable to those studied in rich cluster environments we can perform an important test of the central predictions of hierarchical models of galaxy formation and evolution.

In Section 2 we review the compilation of a spectroscopic sample of 581 luminous field early-type galaxies (Paper I). The star-formation history of the sample, employing both colour-redshift information and spectroscopic diagnostics is investigated in Section 3. In Section 4 we calculate the space density of the galaxies and the paper concludes by considering the implications for models of galaxy formation and evolution in Section 5. Unless otherwise indicated, values of  $\Omega_M = 0.3$ ,  $\Omega_\Lambda = 0.7$  and  $h = H_0/100 \text{ km s}^{-1} \text{ Mpc}^{-1}$  are adopted for the cosmological parameters describing the evolution of a model Friedmann–Robertson–Walker universe.

## 2 THE GALAXY SAMPLE

A full description of the galaxy catalogue employed in this paper is given in Paper I but a summary of the main points is included here for completeness. A total of 9599 objects were selected in an area of  $220 \text{ deg}^2$  spread over 7 United Kingdom Schmidt Telescope (UKST) fields at high Galactic latitude (Paper I; Section 2). The effective area of the survey is  $198.0 \text{ deg}^2$  and the surface density of candidate early-type galaxies at the faint magnitude limit ( $i < 18.95$ ) is  $\simeq 50 \text{ deg}^{-2}$ . Magnitudes, in the natural UKST  $b_{Jori}$  photometric system, calibrated using  $8''$  diameter aperture magnitudes from CCD observations, are available for all objects and satisfy the magnitude and colour selection criteria summarised in Table 1.

The early-type galaxy sample was constructed employing a combination of photometric and morphological criteria. The photometric selection criteria shown in Table 1 were chosen to include the predicted colours of a passively evolving early-type galaxy over the redshift interval  $0.3 < z < 0.55$  while reducing contamination from main sequence K- and M-type stars. Images on each photographic plate were classified as stellar or non-stellar on the basis of a classification parameter (CP) computed from the surface brightness profile (Paper I; Section 2.1). Application

of a suitable rescaling value determined for each plate expresses the CP value as the number of standard deviations separating each object from the centre of the stellar locus. Averaging the individual CP values over all plates on which a particular object is detected then permits robust separation of the stellar locus from the distribution of galaxian objects down to the magnitude limit  $i = 18.95$ . The candidate early-type galaxy sample was constructed by selecting the set of objects that satisfy the photometric criteria described in Table 1 and display CP values  $> 1.5$ . In order to constrain the level of incompleteness in the early-type galaxy sample introduced by these criteria, a sample of candidate stellar objects satisfying the above photometric criteria and  $CP < 1.5$  was also constructed.

Spectroscopy of a sub-sample of  $\sim 600$  galaxies was obtained during 1997–1998 using the Two Degree Field (2dF) facility at the 3.9-m Anglo-Australian Telescope (Paper I; Section 3). The contamination of the sample by stars is extremely small,  $\sim 2\%$ , while the spectroscopic redshift completeness rate, excluding the few stars, is very high  $\gtrsim 95\%$ . Indeed, the majority of the incompleteness in the spectroscopic identifications is due to instrumental or astrometric problems unrelated to the intrinsic nature of the target objects, i.e. close to 100% of the galaxies in the photometric sample are early-type galaxies with redshifts  $0.25 < z < 0.63$ . In addition to observations of early-type galaxy candidates, a sample of 33 stellar candidates were included in the 1998 September 16–17 observations in order to determine directly the level of incompleteness in the early-type galaxy sample. All of the 33 stellar candidates display spectra consistent with that of a K- or M-type star, thus constraining the level of incompleteness in the early-type galaxy sample to  $< 3\%$ .

The total of 581 galaxy redshifts was compiled from a number of observing runs, including some commissioning observations where the data quality was not ideal. In order to ensure a high degree of uniformity the analysis in this paper is confined to 485 galaxies observed in a single two-night run with 2dF on 1998/09/16–17. This sample of 485 galaxies with redshifts is in turn divided into two sub-samples: Sample A, consisting of 371 objects, contains all spectra with reliably determined continuum shapes, and Sample B, consisting of all 485 objects. The necessity for the two sub-samples arose from two factors: the contamination of some of the galaxy spectra by light from an uncovered LED (59 objects) and the identification of a “tail” in the distribution of galaxy continuum spectral properties arising from instrumental/reduction uncertainties (55 objects). The contamination and reduction uncertainties did not impair the assignment of redshifts but the continuum properties of the galaxies so affected are not reliable. The investigation of continuum-dependent properties, such as the generation of the composite spectrum, is confined to the 371 galaxies in Sample A.

A comparison of the effective volume sampled by the spectroscopic early-type galaxy sample to the typical space density of rich galaxy clusters indicates that the early-type galaxy sample described in Paper I is overwhelming drawn from the field. A direct estimate of the effective survey volume is presented in Section 4.2 and is computed as the mean accessible volume for galaxies drawn from spectroscopic sample B occupying the redshift interval  $0.28 < z < 0.6$ .

Comparing the effective survey volume to the observed space density of rich galaxy clusters drawn from a similar redshift interval indicates that the anticipated fraction of cluster early-type galaxies within the sample is  $< 5 - 10\%$ .

One of the principal conclusions of Paper I was that virtually all the galaxy spectra display properties that are entirely consistent with observations of local galaxies (Paper I; Section 4). The composite early-type galaxy continuum is strikingly similar to a local composite early-type galaxy spectral energy distribution (SED) drawn from the atlas of Kinney et al. (1996). However, there are some identifiable differences. Eighty-one objects in Sample A (104 objects in Sample B) possess detectable [OII] 3727 emission (Paper I; Section 4.3) and this sub-sample of galaxies exhibiting detectable [OII] 3727 emission is henceforth referred to as “[OII]-emitting”. The larger sub-sample of galaxies (290 in Sample A; 381 in Sample B) with no detectable [OII] 3727 emission are henceforth referred to as “Normal”. Possible biases against the detection of passively evolving early-type galaxies that have experienced a recent star formation episode are considered in detail in Section 3.2.3. However, the lack of any significant colour differences between the Normal and [OII]-emitting early-type galaxy samples combined with the low star formation rates implied by the observed [OII] 3727 emission fluxes suggests that no significant bias exists. Indeed, the [OII] 3727 emission line luminosity as a function is sufficiently well constrained to reject the existence of a population of intermediate star forming early-type galaxies at the limit of the photometric selection criteria.

The observed number-redshift,  $N(z)$ , distribution of all early-type galaxies with reliable redshifts (Sample B) is consistent with the distribution predicted by applying the survey selection criteria to a model early-type galaxy population described by a representative spectral evolution and luminosity function model of Pozzetti et al. (1996). The extreme range of rest-frame,  $V$ -band, absolute magnitudes present in the sample is  $-22.5 \lesssim M_V - 5 \log h \lesssim -20.5$  with an inter-quartile range of 0.55 magnitudes (Section 4.1).

The early-type galaxy photometry presented in Paper I does not include a correction for Galactic extinction. To facilitate a comparison with recent results in the literature (Section 4.4) extinction corrections from Schlegel, Finkbeiner & Davis (1998) have been made to the galaxy magnitudes. Total to selective extinction values of  $A/E(B - V) = 4.035, 2.649$  and  $1.893$  have been adopted to correct galaxy magnitudes in the  $b_J$ -,  $or$ - and  $i$ -bands respectively.

## 3 STAR FORMATION HISTORY

### 3.1 Colour-redshift evolution

Determining the possible range of age and metallicity consistent with the observed evolution of broad-band colours places important constraints upon the star formation history of the luminosity-weighted stellar population. Most simply, to what extent does the colour-redshift distribution for the galaxy sample conform to the predictions of a single, evolving stellar population model? Additional information is also present in the distribution of galaxy properties, specifically, what are the physical implications of the existence of the galaxy sub-samples, Normal and [OII]-emitting, defined in

Section 2 and how homogeneous are the galaxies within each sub-sample?

The broad-band colours of the galaxy sample are compared to a range of model stellar populations based upon the GISSSEL96 spectral synthesis code (Leitherer et al. 1996). Two fiducial stellar population models are considered; an instantaneous burst and an exponentially decreasing burst of star formation of e-folding time scale  $\tau = 1$  Gyr. Each model is described by a Scalo (1986) Initial Mass Function (IMF) over the mass interval 0.1 to 125  $M_{\odot}$ . The colour-redshift evolution predicted for each model as a function of formation redshift and metallicity is investigated within a spatially flat ( $\Omega_M = 0.3$ ,  $\Omega_{\Lambda} = 0.7$ ,  $h = 0.7$ ) and an open ( $\Omega_M = 0.3$ ,  $\Omega_{\Lambda} = 0.0$ ,  $h = 0.7$ ) model universe. At the median redshift of the galaxy sample ( $\langle z \rangle \simeq 0.4$ ) the age of the universe in the spatially flat and open models is approximately 9 Gyr and 7 Gyr old respectively.

Colour-redshift loci on the  $b_J - or$  versus  $or - i$  plane are compared to observed colour-redshift values via the two-colour probability density function  $G(b_J - or, or - i | z)$  (Appendix A). The function  $G$  describes the two-colour probability density of a simulated population of galaxies at a redshift  $z$ , characterised by a spectro-photometric model computed for a given formation redshift and metallicity, combined with the photometric uncertainties in the  $b_J or i$  passbands. Hence, observed  $b_J or i$  colour distributions are compared to a simulated distribution of galaxy colours described by the formation redshift ( $z_f$ ) and metallicity ( $\log[Z/Z_{\odot}]$ ) of the spectro-photometric evolution model. Following the maximum likelihood technique of Sandage, Tammann & Yahil (1979), one searches for individual values of  $z_f$  and  $\log[Z/Z_{\odot}]$  that maximise the combined probability density for realising the observed galaxy colour-redshift values.

Let  $p(u, v | z)$  be the differential probability density that a galaxy of observed redshift  $z$  will display colours in the interval  $u = b_J - or$  to  $u + du$  and  $v = or - i$  to  $v + dv$ , i.e.

$$p(u, v | z) \propto \frac{G(u, v | z)}{\int_{-\infty}^{\infty} \int_{-\infty}^{\infty} G(u', v' | z) H(u', v') du' dv'}. \quad (1)$$

Where  $H(u, v)$  represents a two-dimensional window function equal to unity when the galaxy colour lies within the colour-selection boundaries (Section 2) and equal to zero when the colour lies outside this region, i.e.

$$\begin{aligned} H &= 1 && \text{if } 2.15 \leq u \leq 3.00 \\ &&& \text{and } 2.95 - u \leq v \leq 1.05 \\ H &= 0 && \text{otherwise.} \end{aligned} \quad (2)$$

Equation 2 describes the case  $E(B - V) = 0$ . For the case  $E(B - V) > 0$ , early-type galaxy  $b_J or i$  photometry and photometric selection limits are adjusted accordingly. The likelihood-term is then constructed from the combination of individual probability density values estimated for the  $k = 1, N$  galaxies in the sample for the given combination of parameters ( $z_f$ ,  $\log[Z/Z_{\odot}]$ ), i.e.

$$\ln \mathcal{L} = \sum_{k=1}^N \ln p(u_k, v_k | z_k) \quad (3)$$

Maximising the likelihood-term over the defined two-

dimensional parameter space equates to determining the most probable combination of input parameters to generate the observed colour-redshift values. Confidence intervals on the returned parameter values may be estimated by determining the surfaces of likelihood defined by the expression

$$\ln \mathcal{L} = \ln \mathcal{L}_{max} - \frac{1}{2} \chi_{\beta}^2(M), \quad (4)$$

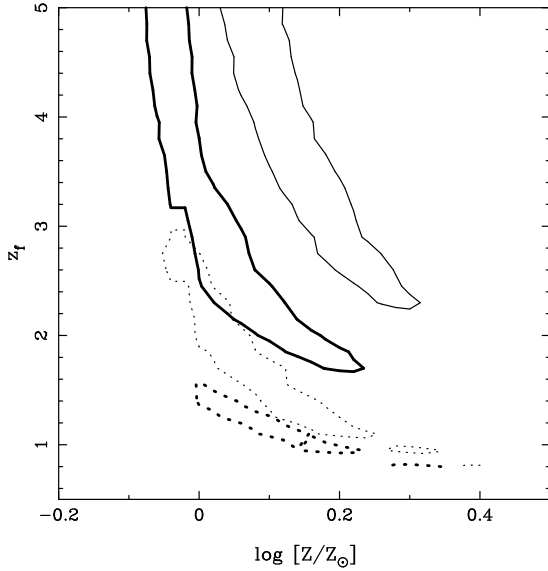
where  $\chi_{\beta}^2(M)$  is the  $\beta$ -point of a  $\chi^2$  distribution with  $M$  degrees of freedom (Efstathiou, Ellis & Peterson 1988). Contours describing a  $4\sigma$  likelihood difference relative to the maximum likelihood value are evaluated. This criterion is adopted to encompass known uncertainties in the optical/infrared colours of evolving galaxies predicted by current population synthesis models (Charlot, Worthey & Bressan 1996). Such likelihood surfaces provide constraints only on the relative likelihood of various parameter combinations.

Figure 1 displays relative likelihood contours in the  $z_f$  versus  $\log[Z/Z_{\odot}]$  plane generated for the Normal galaxy sub-sample. The likelihood contours for each model identify a well-defined locus of star formation scenarios ranging from young, above-solar metallicity stellar populations ( $z_f = 1$ ,  $\log[Z/Z_{\odot}] = 0.2$ ) to old, solar metallicity populations ( $z_f > 3$ ,  $\log[Z/Z_{\odot}] = 0.0$ ). The properties of [OII]-emitting galaxies are statistically identical to the Normal sub-sample; the relative likelihood contours (not shown) are centered on the same region in the projected  $z_f$  versus  $\log[Z/Z_{\odot}]$  plane but extend over a larger area due to the smaller sample size.

Although no colour-magnitude (CM) relation for early-type galaxies has been incorporated, the effect on the analysis is anticipated to be negligible. In their analysis of early-type galaxies in cluster CL 1358+68 ( $z \simeq 0.33$ ), van Dokkum et al. (1998) report a CM-relation  $(B - V)_z = 0.866 - 0.018(V_z - 20.7)$ . At  $z = 0.4$  their redshifted  $B$  and  $V$  bands (i.e. subscript  $z$ ) approximately sample observed frame  $or$  and  $i$ . The absolute  $V$ -magnitude range in our sample is relatively small; the inter-quartile range is 0.54 magnitudes (Section 4.1). Therefore, one anticipates the introduction of an additional dispersion term in the early-type galaxy colours of  $\sim 0.01$  magnitudes, i.e. small compared to the colour distribution resulting from both the observed uncertainties and estimated intrinsic dispersion (see below).

The likelihood contours presented for each model in Figure 1 indicate that the luminosity-weighted stellar populations describing the early-type galaxy sample are consistent with a range of evolving stellar populations where formation redshift, metallicity and/or star formation history vary to some degree. Should the galaxies form over a range of redshifts, then the luminosity-weighted metallicity varies systematically as a function of formation epoch, with more metal rich galaxies formed at later epochs. If star formation history is characterised by a sequence of bursts then shorter bursts are necessary to match the observed colour-redshift distribution at lower redshifts. The constraints on the duration of bursts at high redshift are poor because the colours of stellar populations more than  $\sim 4$  Gyr old are extremely similar. More complex behaviour involving variation of all three model parameters are of course possible.

Ferreras, Charlot & Silk (1999) present a markedly similar result, from a sample of 599 morphologically classified



**Figure 1.** Contours of equal likelihood in the log metallicity,  $\log[Z/Z_\odot]$ , versus formation redshift,  $z_f$ , plane generated from the colour–redshift analysis of the Normal sub-sample. Each contour delineates the  $4\sigma$  likelihood region associated with each model; exponentially declining burst (solid line), instantaneous burst (dashed line), flat universe (heavy line), open universe (light line).

early-type (E/S0) cluster galaxies observed at comparable redshift and luminosity. Their Figure 3(a) may be most directly compared to the instantaneous burst model realised within an open universe presented in Figure 1. The result of Ferreras et al. (1999), and that presented here, indicate that the luminosity-weighted stellar populations of field and rich cluster galaxies were formed over a comparable range of redshift (i.e.  $z > 1$ ) and metallicity ( $\log[Z/Z_\odot] = 0.0 - 0.2$ ).

The observed dispersion of early-type galaxy colours about a given model locus results from the observed photometric uncertainties and from an intrinsic component including some combination of age, metallicity and star formation history variations. The amplitude of the intrinsic dispersion component for a particular colour was estimated by first calculating the expectation value of the distribution of galaxy colour deviations from a given model colour locus, normalised by the photometric uncertainty, i.e.  $\langle F_{\text{colour}} \rangle$ . For example, considering the  $b_J - or$  colour term one writes

$$F_{(b_J - or),k}^2 = [(b_J - or)_k - (b_J - or)_{\text{model}}(z_k)]^2 / \sigma_{(b_J - or),k}^2, \quad (5)$$

for a particular galaxy  $k$  of observed colour  $(b_J - or)_k$ , where  $(b_J - or)_{\text{model}}(z_k)$  is the colour predicted by the selected model locus at the redshift  $z_k$  of the galaxy and  $\sigma_{(b_J - or),k}$  is the observed photometric uncertainty. To simplify the calculation of the colour-deviation statistic, only galaxies that deviate from a particular colour locus in the sense that they fall on the side of the locus opposite to the colour-cut that defines the sample selection are included. This limits the calculation to 270, 261 and 241 galaxies in the  $b_J - or$ ,  $or - i$  and  $b_J - i$  colours respectively, but ensures that the measured dispersions are largely unaffected by the photometric selection criteria (Table 1).

Given the normalised deviation of objects from a particular colour locus averaged across the sample, the “typical” intrinsic contribution per galaxy may be calculated by comparing the observed deviation to the photometric uncertainty for any colour, i.e.

$$\sigma_{\text{int}}^2 = (F\sigma_{\text{obs}})^2 - \sigma_{\text{obs}}^2, \quad (6)$$

where  $\sigma_{\text{int}}$  is the intrinsic colour dispersion and  $\sigma_{\text{obs}}$  is the median photometric uncertainty associated with the selected colour.

Figure 2 compares the intrinsic spread calculated for the  $b_J - or$  versus  $or - i$  plane to colour variations generated by a given stellar population model when varied about central values of formation redshift and metallicity. In addition, the dispersion resulting from varying the assumed star-formation history between an instantaneous burst model and a model employing an exponentially decaying burst of star formation, described by an e-folding time scale of  $\tau = 1$  Gyr, is indicated as a function of formation redshift at fixed metallicity. Figure 2 indicates that the intrinsic colour dispersion observed in the early-type galaxy sample is consistent with only a very modest spread in formation redshift, metallicity or star formation history. For example, the intrinsic colour variations are consistent with an early-type galaxy formation redshift varying over the interval  $2 < z < 3$  at constant metallicity. Conversely, at fixed formation redshift, the intrinsic colour variations are consistent with a metallicity interval  $0.0 < \log[Z/Z_\odot] < 0.2$ . Though more complex scenarios involving the effect of combined variations of formation redshift, metallicity and star formation timescale are also allowed by the data, the low root mean square amplitude of colour variations about a given model locus implies that the early-type galaxy sample describes a predominantly uniform population drawn from a narrow range of intrinsic properties.

## 3.2 [OII] 3727 emission

### 3.2.1 Star formation or active galactic nuclei?

[OII] 3727 emission is detected in 104 galaxies ( $\sim 25\%$ ) of galaxies from Sample B<sup>†</sup> (Paper I; Section 4.3). Star-formation or the presence of an active galactic nucleus could be responsible for the presence of [OII] 3727 emission. Several lines of evidence suggest that the origin of the emission in the majority of galaxies is star formation activity. The majority of active galactic nuclei (AGN) exhibit relatively strong [OIII] 5007, with the flux ratio [OIII] 5007/[OII] 3727  $\gtrsim 3$  (e.g. Baldwin, Phillips & Terlevich 1981). However, a composite spectrum of the 104 galaxies with detectable [OII] 3727 emission shows no evidence for the presence of the [OIII] 4959 5007 doublet or of H $\beta$  in emission. Indeed, in the entire galaxy sample there are no individual detections of [OIII] 5007 or H $\beta$  in emission. The flux limit for detection of [OIII] 5007 in the galaxy spectra is a factor  $\simeq 1.5$

<sup>†</sup> Although the spectra of a small number of galaxies in sample B possess continua that may be affected by contaminating LED emission (Section 2), this does not affect the detectability of [OII] emission and the discussion of the [OII] emission properties is based on galaxies in the larger Sample B.

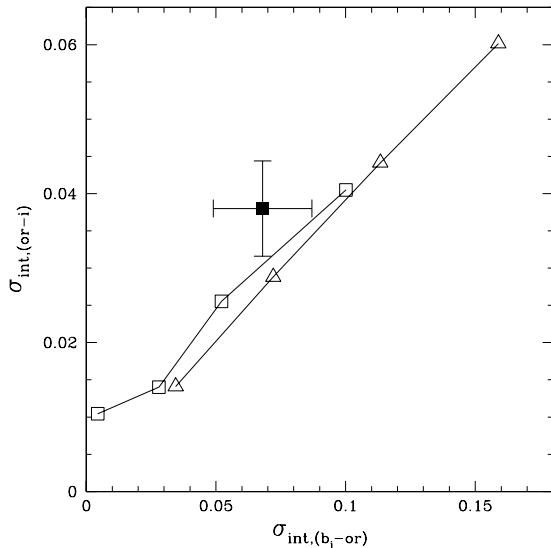


**Figure 2.** Amplitude of intrinsic variation of early-type galaxy colours due to varying model stellar population parameters. The solid square with error bars indicates the intrinsic dispersion values, calculated employing Equations 5 and 6, for the galaxy sample. The extent of the error bars represents the variation in the intrinsic dispersion when the colour errors enclosing 68% of the galaxy distribution about the median value are employed instead of the median value. The fiducial model consists of an exponentially declining burst of star formation of timescale 1 Gyr formed at redshift  $z = 3$  with solar metallicity. Open triangles indicate the colour sequence generated by varying the metallicity of the fiducial model by +0.05, 0.1, 0.15 and 0.2 in log metallicity from bottom left to top right. Open squares indicate the colour variation produced by changing the formation redshift of the fiducial model to  $z = 2.7, 2.4, 2.1$  and  $1.8$ , again, ordered from bottom left to top right. All simulations are considered for a “flat” universe model (see text). All colours are computed for model galaxies at  $z = 0.4$ , the median redshift of the early-type galaxy sample.

poorer than for [OII] 3727, due primarily to the higher sky-background at  $\sim 7000\text{\AA}$ . The lack of detections of [OIII] 5007 is thus surprising if the line ratios were typical of AGN but is entirely consistent with the identification of the source of [OII] emission as low-excitation star formation where the [OIII] 5007/[OII] 3727 ratio is often unity or significantly smaller.

An estimate of the fraction of the galaxy sample hosting AGN can be made from the number of galaxies that are radio sources. The excellent astrometric properties of the galaxy sample (Paper I; Section 2) and the FIRST radio survey (Becker, White & Helfand 1995) allow unambiguous identification of galaxies with radio sources using a matching radius of only 2 arcsec. The FIRST survey includes a significant proportion of the three UKST equatorial fields included in the full photometric catalogue of 9599 candidate galaxies. Of 3170 galaxy candidates within the FIRST survey region, 95 lie within 2 arcsec of a FIRST source. A further 6 galaxies possess multiple FIRST sources, within a 10 arcsec radius, that strongly suggest the galaxy is the origin of radio-lobe emission. Thus, only 101 of 3170 ( $\simeq 3\%$ ) of the galaxies appear to be radio sources to 1 mJy at 1.4 GHz, compared to the much larger percentage showing evidence for [OII] 3727 emission. The FIRST survey does not cover the south-

ern fields where the 2dF spectroscopy was obtained but the NVSS (Condon et al. 1998) extends to declination  $-40^\circ$ , including sources to 2.5 mJy at 1.4 GHz. Unfortunately, the positional accuracy of the NVSS is such that a 15 arcsec pairing radius is necessary when matching the catalogue to the galaxy sample. Comparison of the matches between the galaxy sample and the NVSS and FIRST surveys in the three equatorial regions shows excellent agreement. NVSS includes all but the galaxies corresponding to the faintest FIRST sources with the addition of an extra  $\sim 30\%$  of spurious “matches” due to the much larger pairing radius employed. Applying the same matching radius to the galaxies included in the 2dF spectroscopy produces 14 galaxy–NVSS matches out of 421 galaxies within the NVSS survey area. Ten of the NVSS–galaxy matches are expected to represent physical association, with 4 galaxies paired by chance. The galaxies in the spectroscopic sample thus show a very similar incidence of radio emission to that inferred using the FIRST survey. Of the 14 NVSS matches none are included among the 104 [OII] 3727 emission line objects and the composite spectrum of the 14 objects shows no evidence for any anomalous features. Thus, based on the observed limits to the flux ratio of the [OII] 3727 and [OIII] 4959 5007 emission lines and the small incidence of radio emission among the galaxy sample we conclude that star-formation activity, rather than AGN, is responsible for the majority of the [OII] 3727 emission detected in the galaxy spectra.

### 3.2.2 The [OII] 3727 luminosity function and evolution of the SFR

[OII] 3727 emission arises within HII regions ionised by populations of massive, short-lived O- and B-type stars (Hogg et al. 1998; Osterbrock 1989). Given the short lifetime of such populations ( $\sim 10^6$  yrs), [OII] 3727 emission offers an almost instantaneous snapshot of the current star-formation rate on cosmological time-scales.<sup>§</sup> The luminosity of an [OII] 3727 emission line of flux  $f$  in a galaxy observed using 2dF at redshift  $z$  is

$$L_{[\text{OII}]} = 4\pi d_L^2(z)(f/A), \quad (7)$$

where  $d_L(z)$  is the luminosity distance corresponding to a redshift  $z$  in the specified cosmological model.  $A$  is the fraction of total source flux intercepted by a 2dF fibre. The form of the correction for the fraction of [OII] 3727 emission intercepted by a fibre is based on the assumption that the distribution of continuum and [OII] 3727 emission in the galaxies is co-spatial. The observed emission line fluxes were measured by fitting a Gaussian model to each continuum-subtracted line (Paper I; Section 4.3).

Kennicutt’s (1992) relation, derived from a sample of local galaxies, between mean [OII] 3727 luminosity and star-formation rate (SFR);

<sup>§</sup> While this statement is qualitatively true, the calculation of the true star formation rate requires further information, including the Initial Mass Function. The strength of [OII] 3727 emission resulting from an ionising field is also sensitive to the physical state of the interstellar medium – particularly the electron density and metallicity.

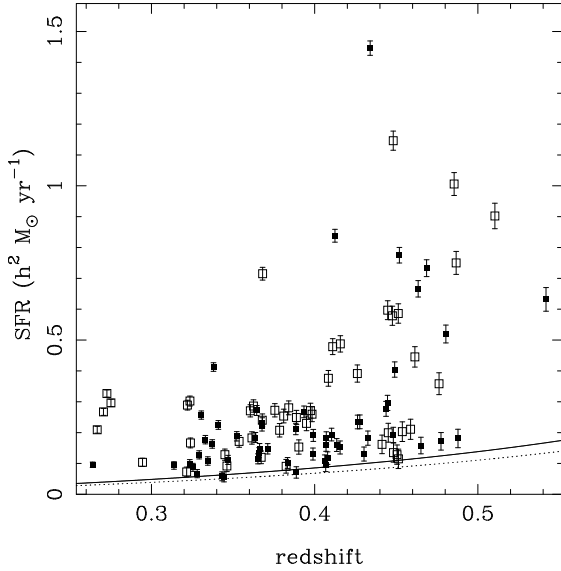


**Figure 3.** SFR, estimated from [OII] 3727 luminosity, versus redshift for 104 galaxies with detectable emission. Open squares represent data obtained on Night 1 (1998/9/16), filled squares represent data obtained on Night 2 (1998/9/17). The solid and dotted lines indicate the detection limit for nights 1 and 2 respectively.

$$\text{SFR}(\text{M}_{\odot}\text{yr}^{-1}) = \frac{L_{[\text{OII}]}}{5 \times 10^{41}} (\text{ergs s}^{-1}). \quad (8)$$

is used to estimate the SFR. [OII] 3727 emission luminosity, rather than [OII] 3727 equivalent width, is employed because, while equivalent width provides a more straightforward indicator of emission relative to the ionising continuum, any sky-subtraction errors introduce significant uncertainties into measurements of equivalent width.

Figure 3 displays the distribution of SFR versus redshift, demonstrating that SFRs inferred from [OII] 3727 luminosities are small ( $\lesssim 1 \text{ M}_{\odot} \text{ yr}^{-1}$ ). The evolution of [OII] 3727 emission, and by implication the SFR, as a function of redshift may be investigated by calculating the [OII] 3727 emission-line luminosity function for the galaxy sample at different redshifts. The nature of the sample is well-suited to the application of the  $1/V_{\text{acc}}$  method (Avni & Bahcall 1980). The maximum accessible volume associated with each [OII]-emitting galaxy in the sample is calculated by integrating the co-moving volume element per unit solid angle,  $dV/dz$ , multiplied by the photometric selection probability as a function of redshift,  $W(z)$  (Equation B4), over the redshift interval within which the estimated [OII] 3727 luminosity exceeds the detection threshold for the identification of [OII] 3727 emission in the galaxy spectrum, i.e.

$$V_{\text{acc}} = c \, d\Omega \int_{z_{\text{min}}}^{z(L_{[\text{OII}]} \geq L_{\text{lim}}(z))} \frac{dV}{dz} W(z) dz, \quad (9)$$

The factor  $d\Omega$  scales the accessible volume by the solid angle covered by Sample B ( $d\Omega \simeq 10.2 \text{ deg}^2$ ) and the factor  $c$  corrects for redshift incompleteness and is equal to the inverse of the redshift completeness rate as a function of apparent  $i$ -magnitude (Paper I; Section 3.5). The cumulative space density of [OII]-emitting galaxies displaying  $L_{[\text{OII}]} > L$ ,

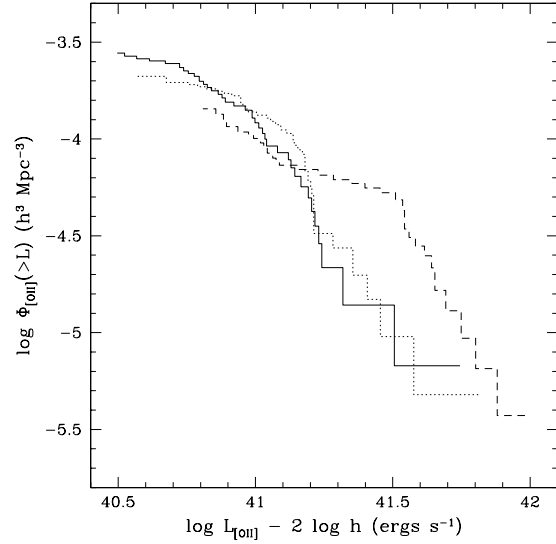


**Figure 4.** Cumulative space density of [OII]-emitting galaxies versus [OII] 3727 luminosity. Data for three redshift shells  $0.28 < z < 0.37$  (solid line),  $0.37 \leq z < 0.43$  (dotted line) and  $0.43 \leq z < 0.6$  (dashed line) are shown.

$\Phi_{[\text{OII}]}(> L)$ , is obtained by summing the inverse accessible volume of each galaxy.

Evolution of the early-type galaxy SFR as a function of redshift was investigated by computing the cumulative space density of [OII]-emitting galaxies as a function of  $L_{[\text{OII}]}$  in three redshift shells ( $0.28 < z < 0.37$  (36 galaxies),  $0.37 \leq z < 0.43$  (32 galaxies), and  $0.43 \leq z < 0.6$  (31 galaxies)), chosen to include approximately equal numbers of galaxies. The photometric selection function was computed employing a model described by exponentially decaying burst of star formation of e-folding time scale  $\tau = 1 \text{ Gyr}$  formed at  $z_f = 3$  with metallicity  $\log[Z/Z_{\odot}] = 0.0$  in a spatially flat universe ( $\Omega_M = 0.3$ ,  $\Omega_{\Lambda} = 0.7$ ,  $h = 0.7$ ). The enclosed volume associated with each [OII]-emitting galaxy,  $V_{\text{enc}}$  (Section 4.2), was also calculated. The resulting cumulative distributions, Figure 4, show a marked increase ( $\Delta \log \Phi \sim 0.5$ ) in the space density of bright ( $L_{[\text{OII}]} > 10^{41} \text{ ergs s}^{-1}$ ) [OII] 3727-emitters at redshifts  $z > 0.43$ . Any difference in the luminosity function between the two lower redshift shells depends on the exact placement of the redshift boundary (at  $z \sim 0.37$ ) and a larger sample is required to draw quantitative conclusions. However, the significant increase in the space density of bright ( $L_{[\text{OII}]} > 10^{41} \text{ ergs s}^{-1}$ ) [OII]-emitters at redshifts  $z > 0.43$  is robust and does not vary significantly as the  $z \sim 0.43$  shell boundary is perturbed.

### 3.2.3 The effect of star-formation on the colour selection

The conclusion that the fraction of early-type galaxies possessing bright ( $L_{[\text{OII}]} > 10^{41} \text{ ergs s}^{-1}$ ) [OII] 3727 emission increases significantly for redshifts  $z \gtrsim 0.4$  is a potentially important result (Section 3.4). However, it is necessary to verify that the presence of star formation activity does not lead to a bias in the selection of galaxies as a function of redshift that might produce a spurious evolutionary trend.

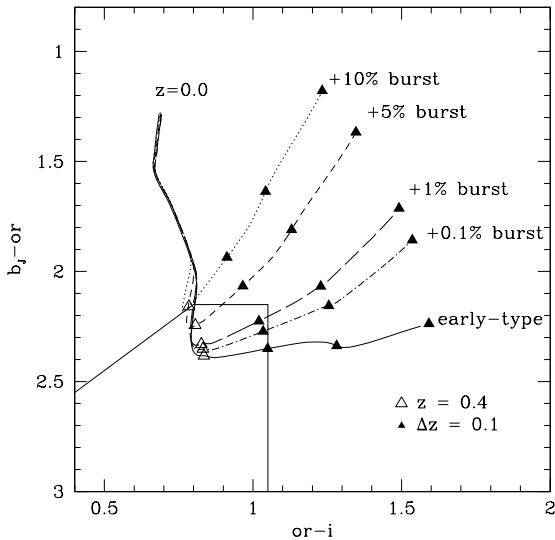


**Figure 5.** Predicted  $b_J - or$  versus  $or - i$  colours as a function of redshift for model early-type galaxies experiencing a star-burst at redshift  $z_b = 1$  (see text for details). Symbols along the tracks are at increments  $\Delta z = 0.1$ . The tracks terminate, on the right, at  $z_{max} = 0.6$ . Note the colour “synchronisation” at  $z \sim 0.3$  for all models.

Consider a galaxy with a passively evolving stellar population formed in an exponentially-decaying burst of star formation ( $\tau = 1$  Gyr), with solar metallicity, initiated at redshift  $z_f = 3$ , that later experiences a burst of star-formation, occurring at  $z_b \sim 1$ . For the adopted cosmological parameters, the age of the burst at the epoch of observation ( $z \simeq 0.4$ ) is 4 Gyr. The star-burst is assumed to involve a population of solar metallicity with a Scalo IMF and an e-folding time-scale  $\tau = 1$  Gyr. Model predictions for mass fractions equal to 10, 5, 1 and 0.1% of the total stellar mass in the galaxy were generated using the GISEL96 code.

Figure 5 shows the predicted behaviour of a galaxy experiencing a burst of star-formation, as described above, in the  $b_J - or$  versus  $or - i$  plane as a function of redshift. Modest star-bursts (0.1% and 1% of the total stellar mass) display colours over the redshift interval  $0.3 \lesssim z \lesssim 0.55$  that are very similar to the underlying model early-type galaxy population ( $\Delta(b_J - or) \lesssim 0.15$ ). More massive star-bursts (5% and 10%) produce markedly bluer colours at redshifts  $z \gtrsim 0.3$ . However, it is a feature of all rapidly fading burst models that optical colours “synchronise” to those of an old stellar population at post-burst ages  $t_b \sim 4-5$  Gyr ( $z \sim 0.25$  within the current model), explaining the tight locus formed by the models at  $z < 0.3$ .

A star-burst at  $z_b \sim 1$  causes the early-type galaxies to become bluer in  $b_J - or$ , moving the galaxies towards the selection boundaries, with the effect most pronounced at the highest redshifts. Thus, any burst of star-formation corresponding to  $\gtrsim 1\%$  of the total stellar mass would result in early-type galaxies at redshifts  $z > 0.4$  becoming lost from the sample. We conclude that the observed increase in the fraction of galaxies with high [OII] 3727 at redshifts  $z \gtrsim 0.4$  is robust and can only increase in the event that a fraction of early-type galaxies experienced massive bursts.

The similarity of the distributions of the Normal and

[OII]-emitting galaxies in the colour-redshift plane, combined with the low-level of the [OII] 3727 emission present, constrains the fraction of the stellar mass involved in a star-burst at  $z_b \sim 1$  for the majority of the sample to be  $\lesssim 0.1\%$ . However, the degree of bluing is a strong function of the mass of the burst and it is not possible to exclude the possibility that some fraction of early-type galaxies experience massive  $\gtrsim 5\%$  bursts of star formation at  $z_b \sim 1$ . Redshift  $z \sim 1$  is the upper limit for which useful constraints may be placed upon star-burst activity using the current sample. Figure 4 illustrates why the signature of bursts occurring at higher redshift are difficult to identify due to the strong degree of colour synchronisation that takes place some 4 Gyr after the bursts. Conversely, the limits on the mass of bursts of star-formation occurring at redshifts  $z \lesssim 1$  are even tighter than the  $\sim 0.1\%$  limit deduced for a burst redshift of  $z_b = 1$ .

### 3.3 Absorption line indices

The measurement of spectral absorption line indices of old stellar populations in early-type galaxies provides a probe of both relative age and metallicity of the luminosity weighted stellar population. Absorption line measures are computed using the Lick/IDS line strength indices (Worthey et al. 1994). The dependence of the Lick/IDS indices, defined by central bandpass and adjacent pseudo-continua, on the age and metallicity of the underlying stellar population have been investigated extensively (Worthey 1994).

Absorption line strengths in the composite spectra of the Normal and [OII]-emitting galaxies were compared. The composite spectrum of each sub-sample was matched to the resolution of Lick/IDS spectra via smoothing with a Gaussian filter of wavelength-dependent FWHM (see Appendix A of Worthey & Ottaviani, 1997). This ensures that the indices measured are on the same scale as those from the Lick/IDS data, to within a small additive constant. The dependence of the indices on galaxy velocity dispersion is also a potential concern. Kuntschner (2000) attempts to correct for galaxy velocity dispersion in the measurement of Lick/IDS indices on early-type galaxies and report corrections  $\lesssim 5\%$  at velocities  $\lesssim 300 \text{ km s}^{-1}$  in the value of the H $\beta$  and C4668 indices employed in this paper (see below). Given that the velocity dispersion correction is small and is difficult to measure accurately without stellar calibration exposures, we do not attempt such a correction here. Errors in the measured absorption indices measured were determined via a bootstrap procedure: absorption indices were measured in composite spectra drawn (with replacement) from the Normal sub-sample. A determination was made for each sub-sample realisation, with the number of galaxies contributing to each realisation equal to the number in each of the galaxy sub-samples. One- $\sigma$  errors were calculated from the resulting distributions of absorption indices measured for 1000 such realisations.

The models of Worthey et al. (1994) predict index values for a passively-evolving, instantaneous-burst stellar population of given age and metallicity. Kuntschner & Davies (1998) advocate the use of the C4668 and Balmer line indices to form a (relatively) independent estimate of the metallicity and age respectively of early-type galaxies in the Fornax cluster. However, they note that galaxy prop-



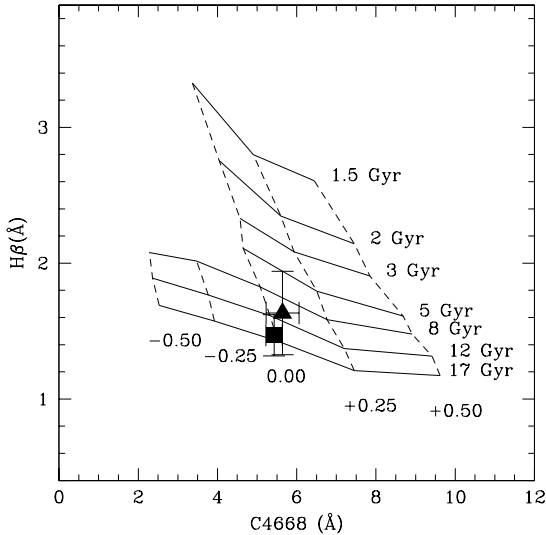


**Figure 6.** Comparison of C4668 and  $H\beta$  Lick/IDS absorption indices measured for the composite spectrum for Normal (square) and [OII]–emitting galaxies (triangle) to indices measured from synthetic stellar populations of varying age and metallicity.  $1\sigma$  errors are derived via a bootstrap analysis (see text). Stellar population predictions are derived from the models of Worthey (1994). Labels placed at the bottom of each grid indicate  $\log[Z/Z_{\odot}]$ , labels placed to the right of each grid indicate stellar population age.

erties inferred from absorption indices should be regarded solely as *relative* measures.

Figure 6 shows the C4668 and  $H\beta$  indices for Normal and [OII]–emitting early-type galaxies drawn from Sample A. The observed offset in the strength of the  $H\beta$  index between the two sub-samples is in the opposite sense to that which would be expected if the [OII]–emitting galaxies exhibited low-luminosity nebular HII emission, effectively reducing the strength of  $H\beta$  in absorption and leading to over-estimation of the apparent age of the galaxy. One may therefore conclude that any offset caused by nebular HII emission in the early-type galaxy sample as a whole is smaller than the estimated error in the  $H\beta$  index determined for the [OII]–emitting galaxies (or alternatively that it is unrelated to [OII] 3727 emission). The absorption line properties of each sub-sample are statistically identical, indicating that the luminosity weighted stellar populations of Normal and [OII]–emitting galaxies share a common star formation history.

### 3.4 Conclusions

To summarise, the mean colour–redshift distribution of the sample is consistent with a luminosity-weighted stellar population that formed at redshift  $z > 1$ . No significant star formation has occurred since that time. If the population formed over an extended period then there must have been a well-defined tight relationship between the mean metallicity of the stars and the formation epoch in order for the galaxy population as a whole to exhibit such a small dispersion in observed properties. The exact relation between formation redshift and metallicity is dependent upon the

assumed star formation rate as a function of time and the cosmological model.

The strength of the mean absorption line indices of both the Normal and [OII]–emitting sub-samples indicates that each sub-sample is consistent with an old ( $\sim 12$  Gyr), approximately solar metallicity ( $\log[Z/Z_{\odot}] \simeq 0.0$  dex) luminosity-weighted stellar population. The results of the colour–redshift and absorption line analyses are consistent and indicate that, modulo the assumed star formation rate as a function of time, the mean luminosity weighted stellar population in luminous field early-type galaxies formed at a redshift  $z \gg 1$  with approximately solar metallicity.

Observation of [OII] 3727 emission in  $\sim 25\%$  of the galaxies indicates that these galaxies are experiencing low SFRs of only  $\lesssim 1 h^2 M_{\odot} \text{ yr}^{-1}$ . This low level of star formation is consistent with the results of the colour–redshift and absorption index analyses that indicate that Normal and [OII]–emitting early-type galaxies possess essentially identical luminosity-weighted stellar populations. The space density of the brightest [OII]–emitting galaxies displays an increase of a factor  $\sim 3$  at the largest redshifts. However, the colour selection criteria that define the sample mean that recent,  $z_b \simeq 1$ , star formation events must involve  $< 0.1\%$  of the total stellar mass of the galaxies.

The conclusions regarding the star formation history of luminous field early-type galaxies appear to be inconsistent with the hierarchical merging of gas rich, massive galaxies at redshifts  $z \lesssim 1$ . Rather, the observations are more consistent with the accretion of gas rich, low mass (presumably dwarf) galaxies leading to a small burst of star formation superimposed upon a dominant, quiescent stellar population. The increase in the space density of the brightest [OII]–emitting galaxies at large redshift may indicate an increase as a function of redshift in the accretion rate of low mass galaxies. However, such a conclusion is critically dependent on the identification of the galaxy population studied here as the progenitors of early-type galaxies today. If in fact the galaxy population studied here represents only a small fraction of the present-day population of early-type galaxies then the conclusions concerning the formation history outlined above could be extremely misleading.

The importance of progenitor-bias in the context of the evolution of early-type galaxies in clusters has been stressed by van Dokkum & Franx (2001). In the context of the sample of field early-type galaxies it is essential to demonstrate that the space density of the population at  $z \simeq 0.4$  is comparable to the space density of early-type galaxies today and this question is addressed in Section 4.

## 4 THE LUMINOSITY FUNCTION

The evolution of the space density of early-type galaxies as a function of redshift places strong constraints upon the extent to which the early-type galaxy population formed via the hierarchical merging of galactic “sub-units”. The 485 galaxies of Sample B allow a direct estimate of the luminosity function at  $z \simeq 0.4$  to be made. A parametric estimator allows a comparison with parametric descriptions of luminosity functions from other samples while a non-parametric estimator provides a direct determination of the luminosity function without the imposition of a possibly inappropriate

model representation. Both types of estimator are employed here.

#### 4.1 Absolute Magnitudes

The analysis of the colour-redshift distributions for each galaxy sub-sample in Section 3.2 demonstrated that the observed colours are consistent with the predictions of a single passively-evolving stellar population model, modulo a small intrinsic dispersion. The effects of passive luminosity evolution over the redshift interval  $0.3 \leq z \leq 0.6$  are significant and the derived rest-frame absolute magnitudes need to be corrected for passive stellar luminosity evolution. In addition, referring luminosity function parameters to a common epoch provides a necessary reference point against which complementary studies of early-type galaxy may be compared. To correct the apparent  $b_{Jori}$  magnitudes of each galaxy to a common epoch it is necessary to compute the apparent magnitude of that galaxy as a function of redshift, i.e.,

$$m_n(z) = m_n - A_n - 5 \log[d_L(z_n)/d_L(z)] - ([e + k](z_n) - [e + k](z)), \quad (10)$$

where each galaxy with magnitude  $m_n$  and redshift  $z_n$  is corrected for Galactic extinction,  $A_n$ , the effect of differential luminosity distance as a function of redshift,  $d_L(z)$ , and a differential evolution plus  $k$ -correction term as a function of redshift  $[e + k](z)$  appropriate to each photometric pass-band. Rest-frame absolute  $V$ -band magnitudes are then determined from apparent  $i$ -band magnitudes computed at a common redshift,  $z_c = 0.4$ , i.e.,

$$M_V = m_n(z_c) - 25 - 5 \log d_L(z_c) - k(z_c) + (V - i)_{z=0.4}, \quad (11)$$

where  $k(z_c)$  is determined from the SED of a  $z = 0.4$  galaxy generated by the specified spectral evolution model and  $(V - i)_{z=0.4}$  is the rest frame  $V - i$  colour for an early-type galaxy at  $z = 0.4$ . Figure 7 shows the absolute magnitude distribution computed for an exponentially decaying burst of star formation of e-folding time scale  $\tau = 1$  Gyr formed at a redshift  $z_f = 3$  with solar metallicity within a spatially flat universe (see Table 2: “Model 2”).

#### 4.2 The luminosity function: $1/V_{acc}$ estimation

In the  $1/V_{acc}$  estimator (Avni & Bahcall 1980) the maximum accessible volume associated with each galaxy in the sample is computed by integrating the co-moving volume element per unit solid angle,  $dV/dz$ , multiplied by the probability that a galaxy of given magnitude and colour enters the sample as a function of redshift,  $W(z)$  (Equation B4), over the specified redshift limits, i.e.

$$V_{acc} = c \, d\Omega \int_{z_{min}}^{z_{max}} \frac{dV}{dz} W(z) dz, \quad (12)$$

The factor  $d\Omega$  scales the accessible volume by the appropriate solid angle and the factor  $c$  corrects for redshift incompleteness. The enclosed volume associated with each galaxy,  $V_{enc}$ , is calculated by replacing the integration limit  $z_{max}$  by  $z_{gal}$ . Redshift limits of  $z_{min} = 0.28$  and  $z_{max} = 0.60$  were

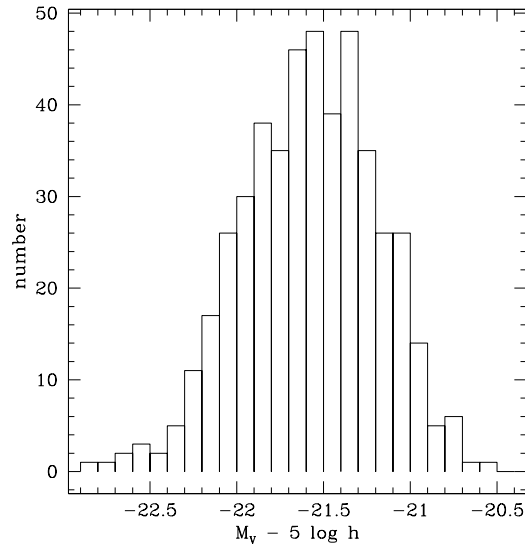


**Figure 7.** Rest-frame absolute  $V$ -band magnitudes, corrected for passive luminosity evolution, at a common epoch,  $z = 0.4$ . See text for discussion.

**Table 2.** Spectral evolution models and cosmological parameters employed in luminosity function analyses. For exponentially decaying star formation histories, the e-folding time scale is set to  $\tau = 1$  Gyr. The “non-evolving” spectral evolution model employs the Kinney SED to determine the  $k$ -correction term. Although  $h$ -dependent values are normalised to  $h = 1$  the adopted value of  $h = 0.7$  determines the age-redshift relation.

Model	Spectral model		Cosmological model		
	SF history	$z_f$	$\log[Z/Z_\odot]$	$\Omega_M$	$\Omega_\Lambda$
1	Instantaneous	1.4	0.0	0.3	0.7
2	Exponential	3.0	0.0	0.3	0.7
3	Non-evolving	—	—	0.3	0.7
4	Instantaneous	2.6	0.0	0.3	0.0
5	Exponential	4.0	0.1	0.3	0.0
6	Non-evolving	—	—	0.3	0.0

adopted to exclude galaxies at redshifts where the probability  $W(z)$  becomes very small. The resulting number of galaxies in the Normal and [OII]-emitting sub-samples were 367 and 99 respectively. The cumulative  $1/V_{acc}$  luminosity function,  $\Phi(< M)$ , is calculated by summing the inverse accessible volumes for each galaxy (Figure 8).

Internal consistency was verified by comparing cumulative luminosity functions for the two sub-samples and for each 2dF field using a two-sample Kolmogorov-Smirnov (KS) test. Figure 8 shows cumulative luminosity functions for the Normal and [OII]-emitting sub-samples together with the combined sample. A KS-test applied to the Normal and [OII]-emitting sub-samples gives  $D_{max}$  and associated probabilities that the samples are drawn from the same distribution, of: (0.11, 0.34), indicating no significant differences.  $D_{max}$  and associated probabilities for samples from each 2dF field compared to the remaining three fields are (0.10, 0.36), (0.13, 0.10), (0.06, 0.90), (0.12, 0.16) for fields 1, 2, 3, and 4 respectively. The sample thus shows no evidence for significant differences in the luminosity function from field to field, although the effects of cosmic variance

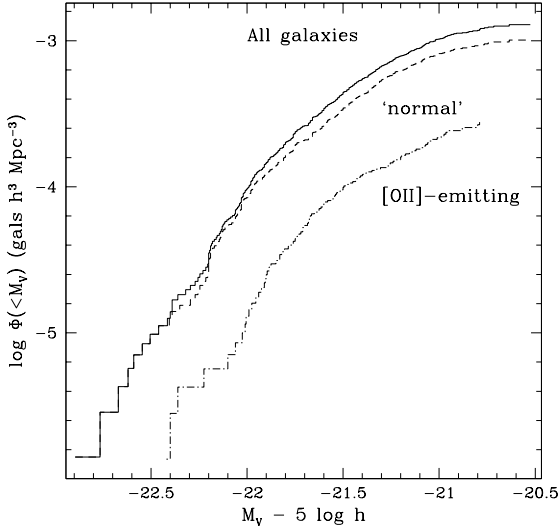


**Figure 8.** Cumulative luminosity functions corresponding to each spectral sub-class compared to the combined galaxy sample. Each luminosity function was generated employing “Model 2”, i.e. an exponentially decaying burst of star formation at  $z_f = 3.0$  with an e-folding time scale of  $\tau = 1$  Gyr within a spatially flat universe.

**Table 3.** Effective spectroscopic survey volume computed for each galaxy formation model presented in Table 2.

Model	$V_{eff} (\times 10^5 h^{-3} \text{Mpc}^3)$
1	7.1
2	7.7
3	6.5
4	5.5
5	5.3
6	4.7

are likely responsible for the smaller probabilities associated with fields 2 and 4.

The effective volume probed by the spectroscopic early-type galaxy sample is computed as the mean accessible volume of all galaxies drawn from Sample B occupying the redshift interval  $0.28 < z < 0.6$ , i.e.

$$V_{eff} = \frac{1}{N} \sum_{i=1}^N V_{acc,i}, \quad (13)$$

where the index  $i$  is summed over the 466 early-type galaxies for which  $V_{acc}$  is computed. Effective survey volumes computed for each galaxy formation model presented in Table 2 are displayed in Table 3. The effective survey volume may be compared to the space density of rich galaxy clusters in order to constrain the contribution of the field early-type galaxy sample by cluster early-type galaxies. The space density of rich ( $R \geq 1$ ) Abell clusters at redshifts  $z < 0.6$  is  $5.6 \times 10^{-6} h^3 \text{Mpc}^{-3}$  (Postman et al. 1996). Comparing this space density to the effective survey volumes for a spatially flat universe indicates that the spectroscopic early-type galaxy sample may contain four rich galaxy clusters. At a redshift  $z = 0.4$ , the photometric selection criteria will sample the cluster early-type galaxy magnitude distribution down to  $\sim m_{10}$  and we therefore assume a cluster contribution rate in the full photometric sample of  $\sim 10\%$ . However,

the strict lower limit on the spatial sampling of galaxy targets imposed by the 2dF instrument (greater than 30 arcseconds) implies that it is unlikely that the presence of a rich cluster in the spectroscopic target fields will contribute more than a few galaxies to the sample. This conclusion is supported by the absence in the spectroscopic sample of any groups of 5 to 10 galaxies within  $2000 \text{ km s}^{-1}$  velocity intervals and within a projected radius of 5 arcminutes – thus implying a cluster contribution rate for the spectroscopic subsample of  $< 5 - 10\%$ .

### 4.3 The luminosity function: the STY maximum likelihood estimator

The STY estimator (Sandage, Tammann & Yahil 1979) is unbiased by density variations and, although the density normalisation is not constrained, the method provides a robust determination of the shape of the luminosity function. The galaxy luminosity function may be defined via the number of galaxies with magnitudes in the interval  $M$  to  $M+dM$  within a volume element  $d\mathbf{x}^3$  to be  $\phi(M, \mathbf{x}) dM d\mathbf{x}^3$ . Based on the results of the previous section we assume that  $\phi(M, \mathbf{x}) = \phi(M)$ , where the given functional form of the luminosity function is characterised by a constant space density  $\phi^*$  per unit volume and magnitude interval. We further assume that the shape parameters describing  $\phi(M)$  do not vary with redshift. Thus, one may express the probability density that a sample galaxy observed at a redshift  $z$  will display an absolute magnitude  $M$  as

$$p(M|z) \propto \frac{\phi(M) f(m) S(z) (dV/dz)}{\int_{z_{min}}^{z_{max}} \int_{-\infty}^{\infty} \phi(M') f(m') S(z') (dV/dz') dM' dz'}. \quad (14)$$

The factor  $S(z)$  describes the colour-redshift selection probability (Equation B1) and  $dV/dz$  is the co-moving differential volume element per unit solid angle. The factor  $f(m)$  indicates the fraction of galaxies entering the early-type galaxy sample as a function of apparent magnitude,  $m$

$$f(m) = 0 \quad \text{where } M > M_{faint}(z) \quad (15)$$

$$\text{or } M < M_{bright}(z)$$

$$f(m) = c(m) \quad \text{where } M_{bright}(z) < M < M_{faint}(z).$$

The factor  $c(m)$  is the redshift incompleteness as a function of apparent magnitude  $m_i$ . The relation between  $m_i$  and rest-frame absolute  $V$ -band magnitudes is given by equations 10 and 11.

The luminosity function is parameterised in terms of a Gaussian distribution of characteristic magnitude  $M^*$  and width  $\sigma_M$ . The photometric errors are incorporated by convolving the intrinsic form of the luminosity function,  $\phi_{int}(M)$ , with a Gaussian function of standard deviation equal to  $\sigma_{obs}$ , the observed  $1\sigma$   $i$ -band magnitude error of each galaxy, to generate an observed luminosity function,

$$\phi_{obs} = \frac{1}{\sqrt{2\pi}\sigma_{obs}} \int_{-\infty}^{\infty} \phi_{int}(M') \exp\left(-\frac{(M-M')^2}{2\sigma_{obs}^2}\right) dM'. \quad (16)$$

The maximum likelihood procedure identifies values of  $M^*$  and  $\sigma_M$  that maximise the log likelihood equation over the  $k = 1, N$  sample galaxies drawn from the redshift interval

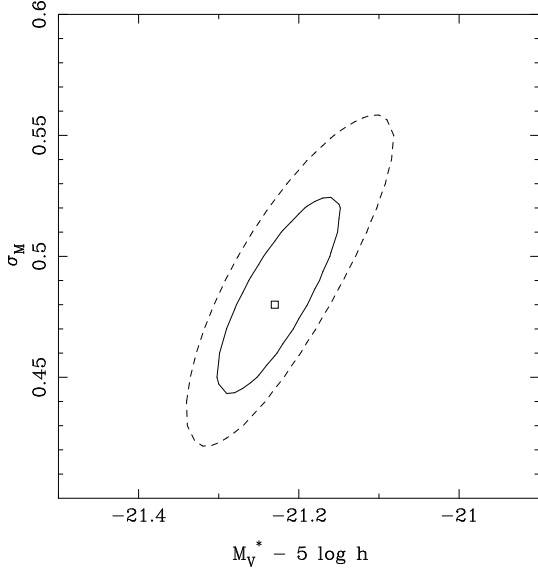


**Figure 9.** Contours of relative likelihood corresponding to 1 (solid) and  $2\sigma$  (dashed) joint error distributions for luminosity function parameters  $M_V^* - 5 \log h$  and  $\sigma_M$ . Contours are computed for Model 1 (Table 4). The open square indicates the formal maximum.

$0.28 < z < 0.6$ , i.e.

$$\ln \mathcal{L} = \sum_{k=1}^N \ln p(M_i | z_i). \quad (17)$$

Confidence intervals in the  $M^*$  versus  $\sigma_M$  may be displayed by computing contours of equal likelihood according to Equation 4. The characteristic density is estimated by normalising the integrated number of galaxies predicted for a given luminosity function model to the total number of early-type galaxies observed in the full photometric sample (Section 2, Paper I; Section 2), i.e.

$$N_{total} = d\Omega \int_{z_{min}}^{z_{max}} \int_{m_{bright}}^{m_{faint}} \phi_{obs}(m(M, z)) \times S(z) (dV/dz) dm dz. \quad (18)$$

The apparent magnitude of an early-type galaxy of absolute  $V$ -magnitude,  $M$  and redshift,  $z$ , is calculated employing Equations 10 and 11 assuming a mean Galactic extinction of  $E(B - V) = 0.0294$ , calculated using the full photometric sample.

#### 4.4 Results and discussion

The results of the maximum likelihood analysis for each spectral evolution and cosmological model combination described in Table 2 are given in Table 4. Figure 9 displays error contours associated with the luminosity function parameters determined for Model 1. Error contours represent the relative uncertainty associated with a given combination of spectral evolution and cosmological model and do not account for uncertainties in the adopted spectral evolution model or cosmological parameters. Errors are thus likely to be underestimated and the luminosity function parameters returned by the maximum likelihood procedure should be

**Table 4.** Gaussian luminosity function parameters estimated via STY maximum likelihood procedure. Parameters are valid over the approximate absolute magnitude interval  $-22.5 < M_V - 5 \log h < -20.5$ . The  $2\sigma$  single parameter errors are  $-M_V^* + 0.11$  for characteristic magnitude and  $\sigma_M + 0.08$  for the width term. The characteristic space density,  $\phi^*$ , is computed via Equation 18 for the central values of  $M_V^* - 5 \log h$  and  $\sigma_M$  determined for each model and is expressed units of  $10^{-3} h^3 \text{ Mpc}^{-3} \text{ mag}^{-1}$ . The  $2\sigma$  uncertainty in the characteristic space density expresses the variation in  $\phi^*$  associated with the corresponding  $2\sigma$  variation in the luminosity function shape parameters. This source of uncertainty dominates over the Poisson uncertainty associated with the photometric sample size.

Model	$-M_V^* + 5 \log h$	$\sigma_M$	$\phi^*$
1	21.28	0.47	$1.50 \pm 0.25$
2	21.23	0.48	$1.46 \pm 0.25$
3	21.28	0.50	$1.59 \pm 0.23$
4	21.12	0.47	$1.86 \pm 0.29$
5	21.10	0.46	$1.96 \pm 0.32$
6	21.10	0.49	$2.17 \pm 0.32$

considered solely as representations of the data over a limited range of absolute magnitude (Lilly et al. 1995). Given the limited range of absolute magnitude and the strong correlation between the errors of the parameters of the Gaussian fit to the luminosity function, the integrated luminosity density is a far more robust quantity. Consideration of the integrated luminosity density has the further advantage that results based on fitting different functional forms for the luminosity function may also be intercompared.

A significant degree of uncertainty can arise when comparing luminosity functions of galaxies defined using different data sets or selected according to different selection criteria. It is necessary to establish both that the same type of objects are included in the determination of the luminosity functions and that the transformations between measured quantities, particularly absolute magnitudes, are well understood. The situation is compounded, as here, when a comparison between luminosity functions of galaxy samples at very different redshifts is attempted. Fortunately, the recent availability of the Sloan Digital Sky Survey (SDSS) Early Data Release (EDR) (Stoughton et al. 2002) and the determination of the luminosity function for early-type galaxies (Eisenstein et al. 2001, Bernardi et al. 2002), allow a relatively direct comparison between our results at  $z \simeq 0.4$  and those pertaining to the present day to be made. Bernardi et al. present luminosity functions in the SDSS  $g^*r^*i^*z^*$  bands for a sample of early-type galaxies with  $\langle z \rangle \simeq 0.1$ . Early-type galaxies within the SDSS are defined according to a combination of morphological (concentration and surface brightness) and spectral (no detectable emission lines and projected velocity dispersion greater than the effective instrumental limit) criteria. The resulting galaxy sample possesses a well-defined mean colour-redshift locus consistent with a uniformly old stellar population, combined with a small Gaussian dispersion about the mean relation. Therefore, in the absence of additional star-formation events, the  $z \simeq 0.4$  early-type galaxy population will evolve passively to form early-type galaxies that satisfy the SDSS selection criteria.

The Gaussian luminosity function parameters of Bernardi et al. in the  $g^*$ -band are transformed to rest-frame

**Table 5.** Luminosity density values calculated for SDSS and  $z = 0.4$  early-type galaxy samples according to Equation 19. Values are expressed in units of  $\times 10^7 h^2 L_{\odot,V} \text{ Mpc}^{-3}$  (see text). The Poisson error for each values is approximately 1%. Note that the SDSS luminosity function values from which the luminosity density is generated are presented by Bernardi et al. for the cosmological model  $\Omega_M = 0.3$ ,  $\Omega_\Lambda = 0.7$  and  $H_0 = 70 \text{ km s}^{-1} \text{ Mpc}^{-1}$ . Hence, for consistency, the SDSS figure is compared only to Models 1–3 described in Table 2.

Model	$\rho_L$	fraction compared to SDSS
SDSS	7.21	–
1	6.87	0.95
2	6.38	0.88
3	7.19	1.00

$V$ -band values at a redshift  $z = 0.4$ . The redshift  $z = 0$   $g^*$ -band characteristic magnitude is corrected for passive luminosity evolution to a redshift  $z = 0.4$  employing the  $Q$ -parameter estimated by Bernardi et al. The zero-point transformation between the  $g^*$ -band absolute magnitudes on the SDSS AB system of Bernardi et al. to those in the  $V$ -band on the Vega system is readily accomplished using the appropriate transmission functions and the early-type galaxy template of Coleman, Wu & Weedman (1980) employed by Bernardi et al. Application of transformations to account for aperture to total magnitudes and a residual zero-point difference result in a total shift of UKST  $i$ -band magnitudes of  $-0.48 \text{ mag}$  relative to the SDSS system (see Appendix C for a comprehensive discussion). The two samples are then compared in terms of the  $V$ -band luminosity density integrated over the common absolute magnitude interval sampled by each survey,  $-23 \lesssim M_V^* - 5 \log h \lesssim -21$ , i.e.

$$\rho_L = \int_{M_{\text{bright}}}^{M_{\text{faint}}} \phi(M) 10^{-0.4(M-M_{\odot,V})} dM, \quad (19)$$

which is expressed in units of  $\times 10^7 h^2 L_{\odot,V} \text{ Mpc}^{-3}$ , assuming that the  $V$ -band absolute magnitude of the Sun is  $M_{\odot,V} = 4.83$ . Comparison of the luminosity density determined for the SDSS and  $z = 0.4$  samples (Table 5) indicates that, within the uncertainties imposed by the spectrophotometric model employed to describe the  $z = 0.4$  early-type galaxy sample and the transformations applied to place the two samples on a common photometric system, there is no significant shortfall in luminous field early-type galaxies at redshift  $z = 0.4$  compared to  $z = 0.1$ .

## 5 DISCUSSION

The properties of luminous, field early-type galaxies at redshifts  $z < 1$  in principle provide an important test of the hierarchical model of galaxy formation. We have presented an analysis of the mean star formation history and space density of a sample of luminous field early-type galaxies selected over the redshift interval  $0.3 \lesssim z \lesssim 0.6$ .

Overall, the mean star formation history of the sample is characterised by an apparently old ( $z_f > 1$ ), solar to slightly above-solar metallicity luminosity-weighted stellar population that has evolved passively since the formation epoch. The colour-redshift evolution, mean absorption line

properties and mean spectrum of the sample present a consistent picture of an old, quiescent stellar population. The exact range of formation redshift and metallicity permitted depends upon the assumed time dependence of the major star formation event and the cosmological model via the look-back time versus redshift relation. The mean properties of the sample are markedly similar to the properties of morphologically-selected luminous elliptical galaxies in rich cluster environments at redshifts  $z < 1$  (Ferreras et al. 1999). Though neither result in isolation constrains the extent to which early-type galaxies in field or cluster environments represent a co-eval or co-metal population, the broad similarity between the star formation history of the dominant stellar mass component in such galaxies is consistent with similar formation conditions for each population.

Approximately one-quarter of the early-type galaxy sample displays detectable [OII]3727 emission consistent with on-going star formation rates  $\lesssim 1.5 h^2 \text{ M}_\odot \text{ yr}^{-1}$ . Consideration of the number redshift distribution of [OII] 3727 emitting galaxies and the effects of a recent burst of star formation upon the colour selection of such galaxies, limits the typical stellar mass content of such star formation events to  $< 1\%$  of the galaxy mass for a burst occurring at redshift  $z = 1$ . However, the space density of the strongest [OII] 3727 emitting galaxies in the sample displays a marked increase at redshifts  $z \gtrsim 0.4$ . Although further detailed observations are required to determine the true nature of such star formation events, the star formation rate associated with each event combined with the increase in space density at higher redshift is consistent with an increasing accretion rate of low mass, gas rich galaxies with increasing look-back time.

Comparison of the luminosity density of the  $z = 0.4$  early-type galaxy sample to the sample of  $z = 0.1$  early-type galaxies from the SDSS shows no evidence of significant change in the luminosity density of luminous field early-type galaxies between these two epochs. In common with results obtained for morphologically selected samples of elliptical galaxies obtained over similar redshift intervals (Schade et al. 1999), these results show no evidence that significant numbers of luminous early-type/elliptical galaxies have formed via merging at redshifts  $z < 1$ . The hypothesis that luminous field early-type galaxies formed via the hierarchical merging of gas rich disk galaxies is not rejected by our results. However, it does seem clear that the bulk of star formation associated with the formation of such galaxies occurred at redshifts  $z > 1$  and the assembly of the most massive early-type galaxies in the field, via any postulated merging process, was largely complete by redshift  $z \simeq 0.5$ .

## ACKNOWLEDGMENTS

JPW acknowledges the support of a PPARC research studentship and financial support from IoA, Cambridge. The project would not have been possible without the data and analysis facilities provided by the Starlink Project which is run by CCLRC on behalf of PPARC. We further thank an anonymous referee for providing a careful and constructive report.

## REFERENCES

- Abraham, R.G., Ellis, R.S., Fabian, A.C., Tanvir, N.R., Glazebrook, K., 1999, MNRAS, 303, 641
- Avni, Y., Bahcall, J. N., 1980, ApJ, 235, 694
- Baldwin, J. A., Phillips, M. M., Terlevich, R., 1981, PASP, 93, 5
- Baugh, C.M., Cole, S., Frenk, C.S., 1996, MNRAS, 283, 1361
- Becker, R. H., White, R. L., Helfand, D. J. 1995, ApJ, 450, 559
- Bernardi, M. et al. 2002, AJ, in press (astro-ph/0110344)
- Bower, R.G., Lucey, J.R., Ellis, R.S., 1992, MNRAS, 254, 601
- Cardelli, J.A., Clayton, G.C., Mathis, J.S., 1989, ApJ, 345, 245
- Charlot, S., Worthey, G., Bressan, A., 1996, ApJ, 457, 625
- Coleman, G.D., Wu, C.C., Weedman, D.W., 1980, ApJS, 43, 393
- Condon, J. J., Cotton, W. D., Greisen, E. W., Yin, Q. F., Perley, R. A., Taylor, G. B., Broderick, J. J., 1998, AJ, 115, 1693
- Dressler, A., Smail, I., Poggianti, B.M., Butcher, H., Couch, W.A., Ellis, R.S., Oemler, A., 1999, ApJS, 122, 51
- Efstathiou, G., Ellis, R.S., Peterson, B.A., 1988, MNRAS, 232, 431
- Eisenstein, D.J. et al. 2001, AJ, 122, 2276
- Ellis, R.S., Smail, I., Dressler, A., Couch, W.J., Oemler, A., Butcher, H., Sharples, R.M., 1997, ApJ, 483, 582
- Ferreras, I., Charlot, S., Silk, J., 1999, ApJ, 521, 81
- Hammer, F., Flores, H., Lilly, S. J., Crampton, D., Le Fevre, O., Rola, C., Mallen-Ornelas, G., Schade, D., Tresse, L., 1997, ApJ, 481, 49
- Heyl, J., Colless, M., Ellis, R.S., Broadhurst, T., 1997, MNRAS, 285, 613
- Hogg, D.W., Cohen, J.G., Blandford, R., Pahre, M.A., 1998, ApJ, 504, 622
- Jørgensen, I., Franx, M., Hjorth, J., van Dokkum, P.G., 1999, MNRAS, 308, 833.
- Kauffmann, G., 1996, MNRAS, 281, 487
- Kauffmann, G., Charlot, S., White, S.D.M., 1996, MNRAS, 283, 117
- Kennicutt, R.C., 1992, ApJS, 79, 255
- Kinney, A.L., Calzetti, D., Bohlin, R.C., McQuade, K., Storchi-Bergmann, T., Schmitt, H.R., 1996, ApJ, 467, 38
- Kuntschner, H., 2000, MNRAS, 315, 184
- Kuntschner, H., Davies, R.L., 1998, MNRAS, 295, 29
- Larson, R.B., 1974, MNRAS, 166, 585
- Leitherer, C. et al. 1996, PASP, 108, 996
- Lilly, S.J., Tresse, L., Hammer, F., Crampton, D., Le Fèvre, O., 1995, ApJ, 455, 108
- Osterbrock, D.E., 1989, Astrophysics of gaseous nebulae and active galactic nuclei, University Science Books, Mill Valley, California
- Pahre, M.A., Djorgovski, S.G., de Carvalho, R.R., 1998, ApJ, 116, 1591.
- Poggianti, B.M., Smail, I., Dressler, A., Couch, W.A., Barger, A., Butcher, H., Ellis, R.S., Oemler, A., 1999, ApJ, 518, 576
- Postman, M., Lubin, L.M., Gunn, J.E., Oke, J.B., Hoessel, J.G., Schneider, D.P., Christensen, J.A., 1996, AJ, 111, 615.
- Pozzetti, L., Bruzual, G., Zamorani, G., 1996, MNRAS, 281, 953
- Sandage, A., Tammann, G., Yahil, A., 1979, ApJ, 232, 352
- Scalo, J.S., 1986, Fundamentals of Cosmic Physics, 11, 1
- Schade, D. et al. 1999, ApJ, 525, 31
- Schlegel, D.J., Finkbeiner, D.P., Davis, M., 1998, ApJS, 500, 525
- Stanford, S.A., Eisenhardt, P.R., Dickinson, M., 1998, ApJ, 492, 461
- Treu, T., Stiavelli, M., Bertin, G., Casertano, S., Møller, P., 2001, MNRAS, 326, 237.
- van Dokkum, P.G., Franx, M., Kelson, D.D., Illingworth, G., Fisher, D., Fabricant, D., 1998, ApJ, 500, 714
- van Dokkum, P.G., Franx, M., Kelson, D.D., Illingworth, G.D., 2001, ApJ, 553, 39
- van Dokkum, P.G., Franx, M., 2001, ApJ, 553, 90.
- Willis, J. P., Hewett, P. C., Warren, S. J., 2001, MNRAS, 325,

1002 (Paper I)

Worthey, G., 1994, ApJS, 95, 107

Worthey, G., Ottaviani, D.L., 1997, ApJS, 111, 377

Worthey, G., Faber, S.M., Gonzalez, J.J., Burnstein, D., 1994, ApJS, 94, 687

Yee, H. K. C., Ellingson, E., Carlberg, R. G., 1996, ApJS, 102, 269

APPENDIX A: MODELING THE DISTRIBUTION OF  $B_JOR I$  COLOURS

For galaxies at a redshift  $z$ , the distribution of  $b_J - or$  versus  $or - i$  colours may be described by a two-dimensional Gaussian function,  $G$ , of the form,

$$G(u, v | z) = \frac{1}{2\pi \sigma_u \sigma_v} \exp \left[ \frac{-(u - u_m)^2}{2\sigma_u^2} \right] \times \exp \left[ \frac{-(v - v_m)^2}{2\sigma_v^2} \right]. \quad (\text{A1})$$

Where

$$u = (or - i) - (b_J - or) \quad (\text{A2})$$

$$u_m = (or - i)_{model}(z) - (b_J - or)_{model}(z) \quad (\text{A3})$$

$$\sigma_u = (2\sigma_{or}^2 + \sigma_{b_J}^2 + \sigma_i^2)^{1/2}$$

and

$$v = (or - i) + (b_J - or) \quad (\text{A4})$$

$$v_m = (or - i)_{model}(z) + (b_J - or)_{model}(z) \quad (\text{A5})$$

$$\sigma_v = (\sigma_{b_J}^2 + \sigma_i^2)^{1/2}.$$

Variables employing the subscript “model” describe the colour of a model early-type galaxy simulated at a redshift  $z$  according to the specified spectro-photometric model. Photometric errors in  $b_Jori$  passbands are denoted by  $\sigma_{b_J}$ ,  $\sigma_{or}$  and  $\sigma_i$  respectively and are assumed to be Gaussian in form (see Paper I; Section 2.1). Figure A1 displays the form of the observed colour density function  $G$ .

## APPENDIX B: THE PHOTOMETRIC SELECTION FUNCTION

The photometric selection function describes the probability that a galaxy of given  $b_Jori$  magnitude and spectral properties described by a suitable spectral evolution model enters the sample selection criteria as a function of redshift. The selection probability,  $S(z)$ , is the probability that a galaxy at a redshift  $z$ , drawn from a simulated galaxy population characterised by the colour-redshift locus computed from the specified spectral evolution and cosmological models together with the photometric errors, will satisfy the sample colour selection criteria (Table 1). Given the distribution of galaxy colours drawn from a simulated population (Appendix A), computation of the photometric selection probability is straightforward, i.e.

$$S(z) = \int_{2.15}^{3.00} \int_{lim(b_J - or)}^{1.05} G(b_J - or, or - i | z) \times d(b_J - or) d(or - i). \quad (\text{B1})$$

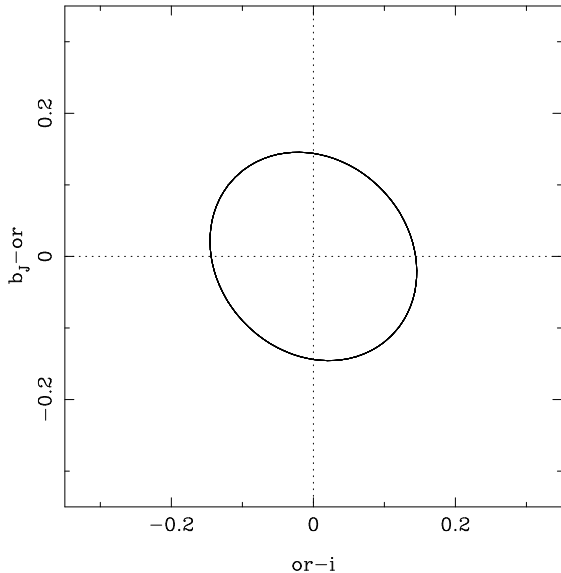


**Figure A1.** Contour describing the  $1\sigma$  probability distribution of  $b_J - or$  versus  $or - i$  colours generated by the colour distribution function,  $G$ , described by the early-type galaxy sample median photometric errors in each passband, i.e.  $\sigma_{b_J} = 0.14$ ,  $\sigma_{or} = 0.08$  and  $\sigma_i = 0.13$  magnitudes respectively.

Where the function  $lim(b_J - or)$  describes the  $or - i$  lower integration limit as a function of  $b_J - or$  colour,

$$lim(b_J - or) = 3.00 - (b_J - or). \quad (B2)$$

The magnitude selection probability as a function of redshift,  $P(z)$ , describes the probability that a galaxy characterised by an apparent  $i$ -band magnitude versus redshift relation,  $m_i(z)$  (Equation 10), and a  $1\sigma$  photometric uncertainty,  $e_i$ , satisfies the magnitude selection threshold (Table 1) at any given redshift, i.e.

$$P(z) = \frac{1}{\sqrt{2\pi}e_i} \int_{16.5}^{18.95} \exp\left(\frac{-(m_i - m_i(z))^2}{2e_i^2}\right) dm_i. \quad (B3)$$

The combined photometric selection function may be expressed as the convolution of the two probability terms, i.e.

$$W(z) = S(z) P(z). \quad (B4)$$

Equations B1–B4 describe the case  $E(B - V) = 0$ . For the case  $E(B - V) > 0$ , early-type galaxy  $b_J or i$  photometry and photometric selection limits are adjusted accordingly.

### APPENDIX C: A COMPARISON OF THE PHOTOMETRIC PROPERTIES OF THE SDSS AND $Z = 0.4$ EARLY-TYPE GALAXY SAMPLES

Any firm conclusions regarding the evolution of the luminosity density of the early-type galaxy population rely critically on understanding the relationship between our sample of galaxies and that of Bernardi et al. (2001). The difficulties inherent in achieving such an understanding are illustrated in the discussion of Eisenstein et al. (2001), particularly §4.2 and Appendix B, in linking the Luminous Red Galaxy (LRG) sample at redshifts  $z \geq 0.3$  to the SDSS MAIN galaxy

sample at lower redshifts. Eisenstein et al. have defined selection criteria designed to achieve the identification of a sample of galaxies complete to a fixed absolute magnitude over an extended range of redshift. However, for practical reasons they are constrained to apparently bright objects, with the result that their absolute magnitude limit corresponds to a point in the luminosity function where the number of galaxies is rising extremely rapidly. Our sample, defined using straightforward apparent magnitude and colour cuts, does not possess the desirable property of probing an absolute magnitude range independent of redshift (Paper I; Figure 19). On the other hand the sample extends sufficiently faint that, for redshifts  $z \lesssim 0.5$ , the absolute magnitude range extends into a much flatter portion of the luminosity function. Specifically, our magnitude limit corresponds on the SDSS system to  $r_{Petro}^* \simeq 19.9$  compared to the (main) Cut I of  $r_{Petro}^* \simeq 19.2$  and Cut II of  $r_{Petro}^* \simeq 19.5$  employed by Eisenstein et al.. Thus, our sample, while not probing to fixed absolute magnitude independent of redshift, includes a much larger fraction of the early-type galaxy population and does not involve a selection cut falling in a steeply rising portion of the luminosity function.

The SDSS EDR contains objects in  $\sim 12 \text{ deg}^2$  areas in two of the seven United Kingdom Schmidt Telescope (UKST) survey fields that make up our full photometric sample (Paper I). The overlap between the two samples allows a direct comparison of the properties of  $\sim 1000$  objects in common and also provides an empirical determination of the transformation between the SDSS photometric system and the natural UKST system employed throughout this paper.

The range of  $g^* - r^*$  and  $r^* - i^*$  colours for the 1014 objects in common in the F855 and F864 fields are statistically indistinguishable from the subset of galaxies that are actually included in the Eisenstein et al. LRG. There is a similarly encouraging agreement in the selection-colour ( $c_{par}$ ) versus  $r_{Petro}^*$  parameter-space (Eisenstein et al.; Figure 3), with an essentially one-to-one correspondence between objects satisfying the LRG selection criteria and those in our sample for magnitudes  $r_{Petro}^* \lesssim 18.7$ . Our simpler colour-selection criteria corresponds to a closer to horizontal boundary in  $c_{par}$  for magnitudes  $18.7 \lesssim r_{Petro}^* \lesssim 19.2$  and additional (intrinsically fainter at given redshift) galaxies in our sample lie approximately 0.1 mag bluer in  $c_{par}$  in the faintest half-magnitude of the Eisenstein et al. Cut I selection.

The morphological properties in the SDSS of the 1014 objects in common are very encouraging. Less than  $< 3\%$  of the objects are classified as stellar or indeterminate and 85% of the sample are “best-fit” by a de Vaucouleurs profile.

The magnitude zero-points used for the sample of early-type galaxies described in Paper I were determined using CCD observations of galaxies measured within 8 arcsec diameter circular apertures. However, SDSS early-type galaxy magnitudes are presented as “total” magnitudes obtained by integration of a de Vaucouleurs surface brightness profile determined for each galaxy. Therefore, a correction must be applied to transform the 8 arcsec early-type galaxy magnitudes presented in this paper to “total” magnitudes. An empirical determination of the difference between the SDSS EDR model “total” and 8 arcsec diameter aperture magnitudes for the  $\simeq 1000$  galaxies in common gives a me-

dian difference of 0.32 mag in the SDSS  $i^*$ , i.e., the “total” magnitudes are 0.32 mag brighter than the aperture magnitudes and the magnitudes in Paper I should be corrected brightward by this amount. Both SDSS and  $z = 0.4$  early-type galaxy magnitudes have been corrected for Galactic extinction using the maps of Schlegel et al. (1998).

Finally, following the transformation of the two samples onto a common magnitude system, i.e., either Vega-based or ABmag-based, it is possible to compare the magnitude scales of the galaxies in the two samples. Specifically, the information available in the SDSS EDR for the galaxies in common can be used to derive 8 arcsec diameter aperture magnitudes to be compared to our magnitudes, also based on 8 arcsec diameter measurements. The comparison for the SDSS  $r^*$  and our  $or$  values is excellent. The median difference between the magnitudes (transformed to a consistent system) is +0.02 mag in the sense that our  $or$  magnitudes are fainter than the SDSS values. The offsets for the two independent fields, F855 and F864, are also in good agreement. Considering the same comparison for the SDSS  $i^*$  and our  $i$  magnitudes also produces excellent agreement between the two independent fields but the median magnitude difference is +0.16 mag, again in the sense that our magnitudes are fainter than the SDSS values. This, well-determined, offset in the magnitudes is uncomfortably large. Eisenstein et al. discuss the question of residual uncertainties in the zero-points of the SDSS photometric bands and conclude that there could be errors in the preliminary calibrations of the SDSS bands, but it seems very unlikely that such errors would exceed 0.05 mag in the SDSS  $i$ -band. Our own zero-pointing procedure (Paper I; §2.2) is uncertain to  $\simeq 0.05$  mag and a systematic error of  $\simeq 0.1$  mag is not out of the question. However, the difference of +0.16 mag appears large given the quoted uncertainties and we have no entirely satisfactory explanation for the difference. The difference in the  $i$ -band magnitude scale is particularly important because our absolute magnitudes are calculated using the  $i$ -band apparent magnitudes. Ideally, it is desirable to undertake absolute determinations of luminosity functions at different redshifts, but in practice the question of whether there has been any significant evolution of the luminosity function with redshift relies on a differential measure. Thus, when comparing our determination of the luminosity density of early-type galaxies at  $z \simeq 0.4$  to that at lower redshifts from Bernardi et al. we will use a value calculated using  $i$ -band magnitudes shifted brightward by 0.16 mag.

To place the SDSS and  $z = 0.4$  early-type galaxy samples on a common photometric scale, we therefore apply a global shift of  $-0.48$  mag to all early-type galaxy UKST  $i$ -band magnitudes.

This paper has been produced using the Royal Astronomical Society/Blackwell Science L<sup>A</sup>T<sub>E</sub>X style file.